Wear xxx (xxxx) xxx

Contents lists available at ScienceDirect

Wear

journal homepage: http://www.elsevier.com/locate/wear

Experimental and modelling study of the effect of martensite volume fraction on friction and wear of dual-phase steel at microscopic scale

C. Penfornis, A. Jourani *, P.-E. Mazeran

Université de technologie de Compiègne, Roberval (Mechanics Energy and Electricity), Centre de recherche Royallieu, CS 60319 - 60203, Compiègne, Cedex, France

ARTICLE INFO

Keywords:
Dual-phase
Nanoindentation
Abrasion
Scratch

ABSTRACT

In this work, the influence of martensite volume fraction, load and attack angle on hardness, friction and wear of ferrite and martensite phases of a dual-phase microstructure is investigated through nanoindentation and scratch tests with conical tips. Friction coefficient increases with the attack angle and is always higher for ferrite than for martensite. For martensite phase, friction coefficient increases and wear resistance decreases as martensite volume fraction increases. As the attack angle increases, wear mechanism changes from ploughing to cutting for martensite. Experimental results correlate to the Axén & al. approach based on the Equal Pressure model.

1. Introduction

Abrasive wear is well studied for homogeneous materials [1–3]. The main material property that characterize the wear resistance of material is its hardness. Moreover, the shape of the abrasive particles and the load are also of great importance to characterize the friction coefficient, defined as the ratio of the tangential to the normal load [4–9], the wear rate, which is generally represented by the Archard's equation [10], and the abrasive wear mechanisms: ploughing, wedging or cutting [11–13].

On the other hand, a complete understanding of the friction and wear behavior of multiphase materials is still lacking due to the complex interactions between the abrasive surface and the inhomogeneous surface properties. Dual-phase steels are an example of such complex materials. Their microstructure benefits from the hardness of martensite and the ductility of ferrite, giving to dual-phase microstructure a better wear resistance than fully martensitic microstructure. They are very useful in the automotive industry to manufacture high strength sheets with good formability and in mining or mineral processing as wear resistant materials.

Numerous works have studied the tribological properties of dual-phase steels [14–23]. However, most of the studies remain on the macroscopic scale and do not relate the tribological behavior of the dual-phase steel to the individual phase properties of the ferrite and martensite. Recently, Trevisiol & al. have realized pin-on-plate abrasive tests on 25CD4 low alloy steel [16–18]. They have shown that various microstructures with the same chemical composition and macro-hardness but different morphologies have different friction and wear behaviors. It is clearly demonstrated that macro-hardness is not sufficient to explain tribological properties of dual-phase microstructures. Consequently, a detailed study of ferrite and martensite individual friction and wear properties is needed to fully understand the macro-scale tribological behavior of dual-phase steels.

This work proposes a study of the mechanical and tribological properties of the ferrite and martensite phases in dual-phase microstructures prepared with martensite volume fraction from 48% to 100% from a 25CD4 low alloy steel. First, the hardness of ferrite and martensite phases are measured by instrumented nanoindentation and analyzed individually. The identification of an indentation size effect allows for the calculation of the macro-hardness of each samples. A comparison between macro-hardness obtained from Oliver & Pharr nanoindentation analysis, Loubet nanoindentation analysis and Vickers microhardness is realized. Martensite and ferrite phases hardness are related to macro-hardness through an inverse rule of mixture.

In a second part, scratch tests with conical tips of attack angles ranging from 18° to 55° are realized under loads from 20 mN to 200 mN to correlate friction and wear properties of both phases with their composition and hardness. Some authors have already realized scratch tests on dual-phase steels with sphero-conical tips with radius of several micron [24,25]. In order to precisely study the effect of the attack angle on each phase, tips with almost perfect conical shape are used. Moreover, the geometries of the conical tips are carefully measured to take into account the tip defects in the analysis. Then, friction coefficient, wear resistance and wear mechanisms are studied independently on ferrite and martensite.

* Corresponding author.
E-mail address: abdeljalil.jourani@utc.fr (A. Jourani).

https://doi.org/10.1016/j.wear.2021.203878
Received 12 November 2020; Received in revised form 11 March 2021; Accepted 15 March 2021
Available online 25 March 2021

This study focuses on the friction and wear behavior of the microstructure in its 'virgin' state from only one scratch test. Then, the results are expected to be different from a practical situation where a steady-state is attained after some run-in time. Further work will have to study the evolution of the tribological behavior of the phases from run-in time to steady-state through multiple scratch tests.

Finally, the models for friction and wear of multiphase materials proposed by Axén & al. are adapted to dual-phase steels [26,27]. An improvement is realized by taking into account the variations of the properties of martensite and ferrite with martensite volume fraction for each attack angle and load. It is shown that the macroscopic behavior from the equal pressure hypothesis is obtained from the implementation of the microscopic behavior of the phases.

2. Experimental procedure

2.1. Material and heat treatments

The material used in this study is a 25CD4 low alloy steel whose nominal composition is detailed in Table 1. Samples are cut from an initial rod of 16 mm in diameter before being subjected to heat treatment.

Heat treatments are done to generate one fully martensitic microstructure and four ferrite-martensite dual-phase microstructures with various volume fraction of martensite. The description of a typical step quenched heat treatment is given in Fig. 1.

The heat treatments are realized as follows. First, the samples are austenitized at 900 °C for 30 min. Then, the first sample is quenched in water to obtain a fully martensitic microstructure while the others are held at an intercritical annealing temperature of 725 °C for various time before water quench. During the intercritical annealing, ferrite grains nucleate and grow at austenite grain boundaries. The remaining austenite is transformed into martensite during the water quench. The fraction of ferrite formed increases with the intercritical annealing time. In the end, the resulting microstructures are composed of ferrite and martensite, forming dual-phase microstructures DP-48% to DP-88%.

After heat treatments, the five samples are mechanically polished with SiC papers of grit ranging from 80 to 4000. The finishing is done with diamond paste of 3 µm and 1 µm. Then, the samples are cleaned by ultrasound with ethanol for 10 min.

In order to measure the martensite volume fraction, the samples are observed with a Field Emission Gun-Scanning Electron Microscope (FEG-SEM) ZEISS Sigma using a Back Scattering Electron (BSE) detector at 20 keV. The BSE detector is used in this study because it allows to distinguish ferrite from martensite without etching the surface. Indeed, the different composition and crystallographic structure of both phases create a chemical contrast when observed with BSE detector. This property is used first to determine the martensite volume fraction of the dual-phase microstructures and then for the non-destructive observation of the wear mechanisms in each phase after the scratch tests have been realized. Finally, the martensite volume fraction of the four dual-phase microstructures are measured by image processing of SEM images of at least five different locations on each sample using ImageJ software.

Because carbon concentration in ferrite is limited to 0.02%wt, the carbon content in martensite will vary with martensite volume fraction. Indeed, during the intercritical annealing, while the fraction of the ferritic phase increases, the carbon is forced to diffuse in the remaining austenite, increasing the carbon content of the subsequent martensite. A rule of mixture can be used to calculate the carbon content of the martensitic phase C_M in dual-phase steels as function of the global carbon content of the steel C, the martensite volume fraction α_M and the ferrite carbon content C_F:

$$C = \alpha_M C_M + (1 - \alpha_M) C_F \quad (1)$$

For 25CD4, the global carbon concentration is C = 0.25%wt. Then for martensite volume fraction α_M going from 48% to 100%, the martensite carbon content decreases from 0.5%wt to 0.25%wt. Heat treatments parameters, resulting martensite volume fraction and theoretical carbon content of martensite in each sample are given in Table 2.

Table 1
Chemical composition of 25CD4 low alloy steel.

	C	Si	Mn	P	S	Cr	Mo
%WT	0,25	<0,4	0,65	<0,035	<0,035	1,15	0,2

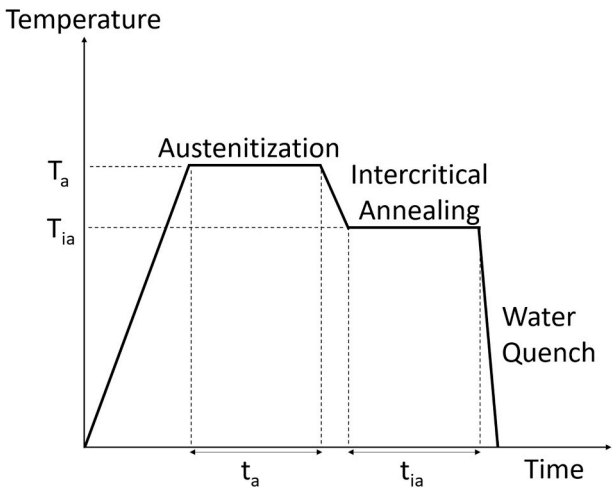

Fig. 1. Schematic drawing of the performed step quenched heat treatment.

2.2. Hardness measurements

Hardness characterization of the microstructures is realized by instrumented nanoindentation with a Nanoindenter Agilent G200 from Keysights Technologies and a diamond Berkovitch tip. At least 90 indentations with a spacing of 100 µm between each others are done on each sample. Calculation of hardness as function of the depth of indentation are done from Continuous Stiffness Measurements (CSM) data. Maximum load for each test is 630 mN and specific values at a given depth or load are then extracted from the CSM data acquired during the loading part of the test.

Two methods of analysis are used and compared. The first one is the well-known Oliver and Pharr method [28] for which the contact depth and the contact area A_c are calculated from:

$$h_c = h - \varepsilon L/S \quad (2)$$

$$A_c = C_0 h_c^2 + C_1 h_c \quad (3)$$

where h is the measured depth, L the load, S the contact stiffness, ε a coefficient equal to 0.75 for a Berkovitch tip. $C_0 = 24.735$ and $C_1 = 2750$ are coefficients calibrated for the Berkovitch tip used in this study.

The second method is the one proposed by Loubet [29], for which the contact depth h_c and the contact area A_c are calculated as follows:

$$h_c = \alpha(h - L/S - h_0) \quad (4)$$

Table 2
Heat treatment parameters and corresponding martensite volume fraction αm for the five samples.

Sample	T_a (°C)	t_a (min)	T_{ia} (°C)	t_{ia} (min)	α_m (%)	C_m (%wt)
M-100%	900	30	–	–	100 ± 0	0,25
DP-88%	900	30	725	3	88 ± 2	0,28
DP-81%	900	30	725	4	81 ± 3	0,30
DP-66%	900	30	725	7	66 ± 3	0,37
DP-48%	900	30	725	10	48 ± 2	0,50

$$A_c = 24.5h_c^2 \quad (5)$$

where h_0 is the tip defect whose value is 55 nm in this study and α a coefficient equal to 1.2. Then, the hardness H is calculated as:

$$H = L/A_c \quad (6)$$

From the calculation of hardness as function of depth of indentation, an Indentation Size Effect (ISE) is identified and fitted with the model of Nix and Gao [30] which relates the hardness H measured at a depth of indentation h to the macro-hardness H_0 and a characteristic length h* through:

$$H \Big/ H_0 = \sqrt{1 - h^*/h} \quad (7)$$

Finally, Vickers micro-hardness with a load of 20 N are realized. The average of five measurements are compared to the macro-hardness fitted from the ISE by both Oliver and Pharr method and Loubet method.

In order to identify the hardness of each phase separately, the value of hardness at a depth of indentation of 200 nm is used. Indeed, at this depth, the area of the imprint is of the order of 1 μm^2 and should be poorly influenced by the surrounding phases. Fig. 2a) shows all the hardness curves realized on the DP-88% sample as an example. At 200 nm in depth, the curves that are below 5 GPa are considered to be ferrite while those above 7 GPa are considered to be martensite. Between 5 and 7 GPa, the phase is considered as undetermined. Then, the value of hardness for each phase at a given load is taken as the mean of all corresponding curves at this load. Fig. 2b) and c) show two examples of imprints remaining after a maximum load of 630 mN, the first one on a martensite grain and the second one on the ferrite grain. The size of the imprint when the depth of indentation is of 200 nm is also represented.

2.3. Scratch tests and tip geometry

Scratch tests are realized on the same nanoindenter used in scratch mode under constant normal loads of 20, 50 or 200 mN. The scratch length is set to 500 μm and the scratch velocity is set to 50 μm/s. For each scratch test, a profile over the entire wear track on the original surface is done under a load of 50 μN. Then the indenter returns to the origin and performs the scratch under the imposed normal load. For each scratch test, the normal load, the tangential load and the scratch depth are measured as function of the scratch length.

In order to study the effect of the attack angle of the asperities, four conical tips are used. A proper measurements of the geometry of the tips is necessary to make sure that the conical geometry is respected even at low load. For this purpose, indentations on an eutectic 63%Sn-37%Pb sample have been realized with the four conical tips and the topography of the prints were measured with a Bruker's Dimension Icon Atomic Force Microscope. Then, the mean profiles for each tip has been extracted from the topography and the mean attack angles have been measured. Full lines in Fig. 3 represent the averaged profiles extracted from the topographies of each tip. Dotted lines are the slopes of the conical geometry of the tips from which are calculated the attack angles β. Deviations from perfect conical tips are observed for depth below 1 μm.

The friction and wear on each phase is identified thanks to the depth and friction profile. An example is shown on Fig. 4 for scratches realized on the DP-48% sample under a load of 50 mN and with each four conical tips. The phases are identified on the depth profile: martensite corresponds to the higher values (higher hardness) while ferrite corresponds to the lowest values (lower hardness). Then, the friction coefficient corresponding to the same positions on the scratch length is attributed to each phase.

3. Experimental results: microstructure, friction coefficient, specific wear resistance and wear mechanisms

3.1. Microstructure and hardness characterization

Scanning electron micrographs of the five microstructures are shown in Fig. 5. We can observe for all microstructure that martensite is formed inside prior austenite grain in the shape of parallel laths regrouped into packets. For samples DP-48% to DP-88%, the dual-phase microstructures are composed of coarse grains of martensite surrounded by ferrite.

In order to characterize the mechanical properties of the martensite and ferrite phases, instrumented nanoindentation has been realized on each sample and analyzed as detailed in section 2.2. Hardness of each indentation is calculated from load, depth and stiffness data with both methods of Oliver and Pharr [28] and Loubet [29] for comparison purposes. First, ferrite and martensite hardness are studied separately as function of the martensite volume fraction and the load. Then, an analysis of the macro-hardness is realized to compare the samples with each other. Then, the macro-hardness of each sample is related to the

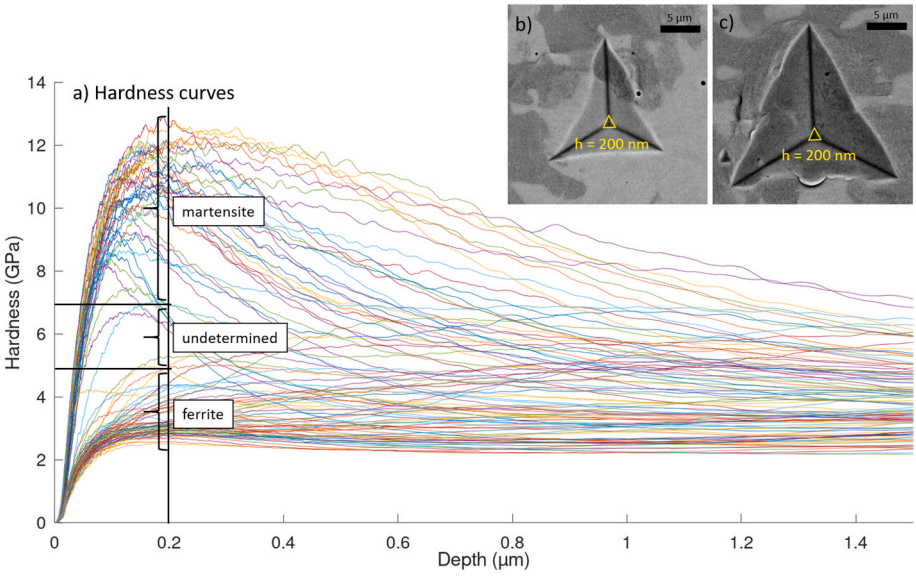

Fig. 2. a) Hardness curves for all tests on the DP-48% samples and criteria for identification of martensite and ferrite and example of remaining prints after full load of 630 mN on b) a martensite grain and c) a ferrite grain with the size of the indentation at h = 200 nm.

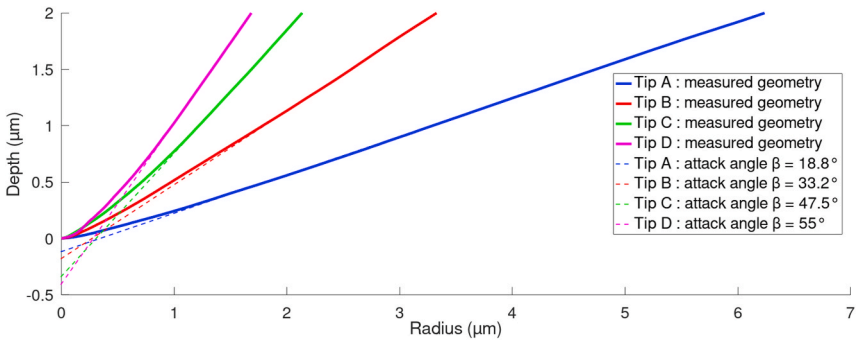

Fig. 3. Mean profiles and mean attack angles for the four conical tips.

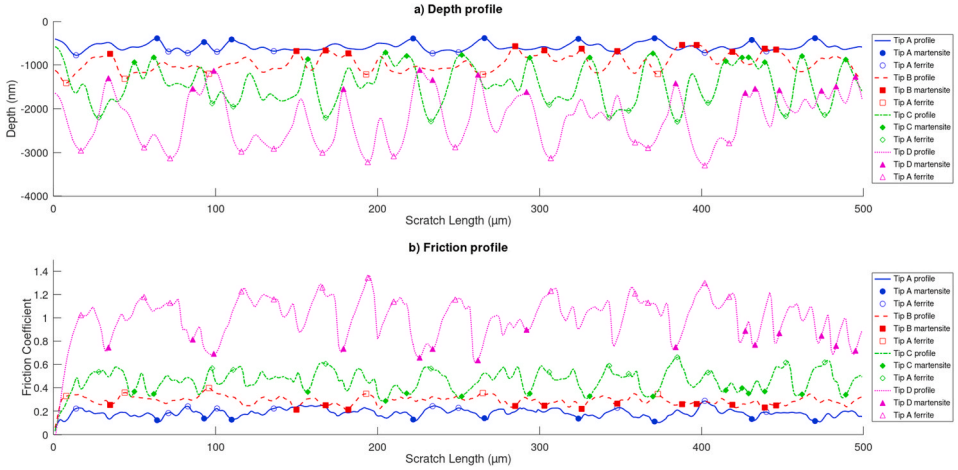

Fig. 4. a) Depth profiles and b) Friction profiles for scratches realized on DP-48% samples under load of 50 mN with the four conical tips. Points identified as martensite are represented as full markers and those identified as ferrite are shown as empty markers.

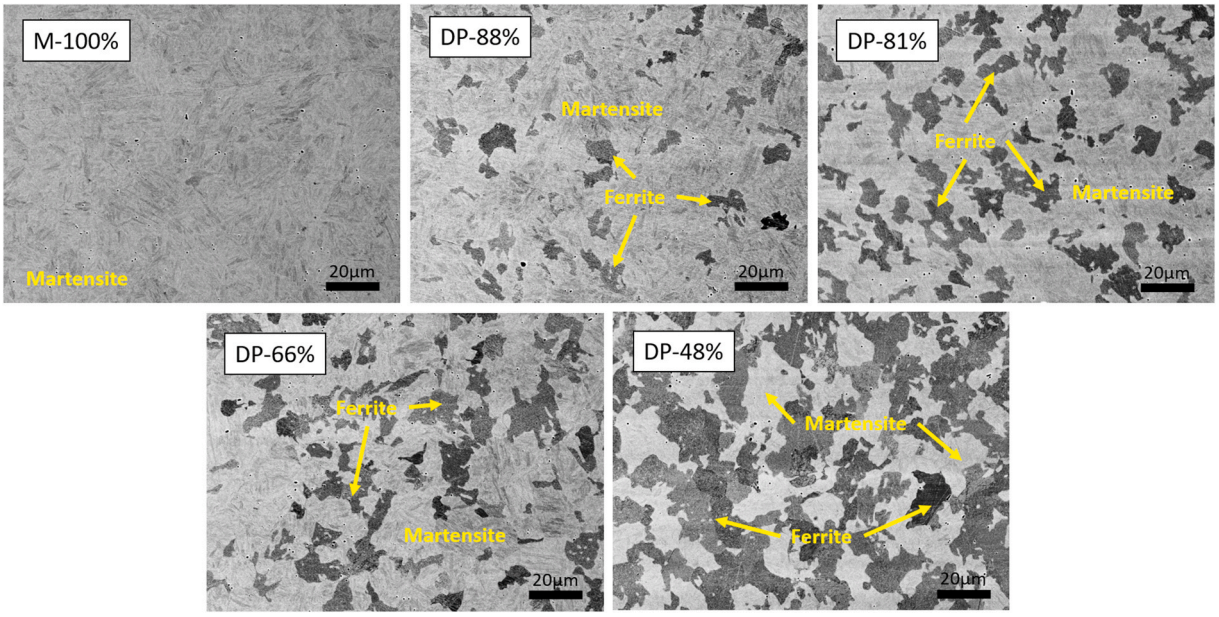

Fig. 5. SEM images for the five generated microstructures. Martensite appears bright and ferrite appears dark.

ferrite and martensite hardness and martensite volume fraction.

Fig. 6 presents the evolution of martensite, ferrite and mean hardness calculated from Loubet analysis as function of the martensite volume fraction at loads of 20, 50 and 200 mN. At 20 mN, martensite hardness decreases when the martensite volume fraction increases while it is constant at 200 mN. No significative change is observed for ferrite hardness, except for a small increase on the DP-88% sample where ferrite grain size is the smallest and the hardness is probably influenced

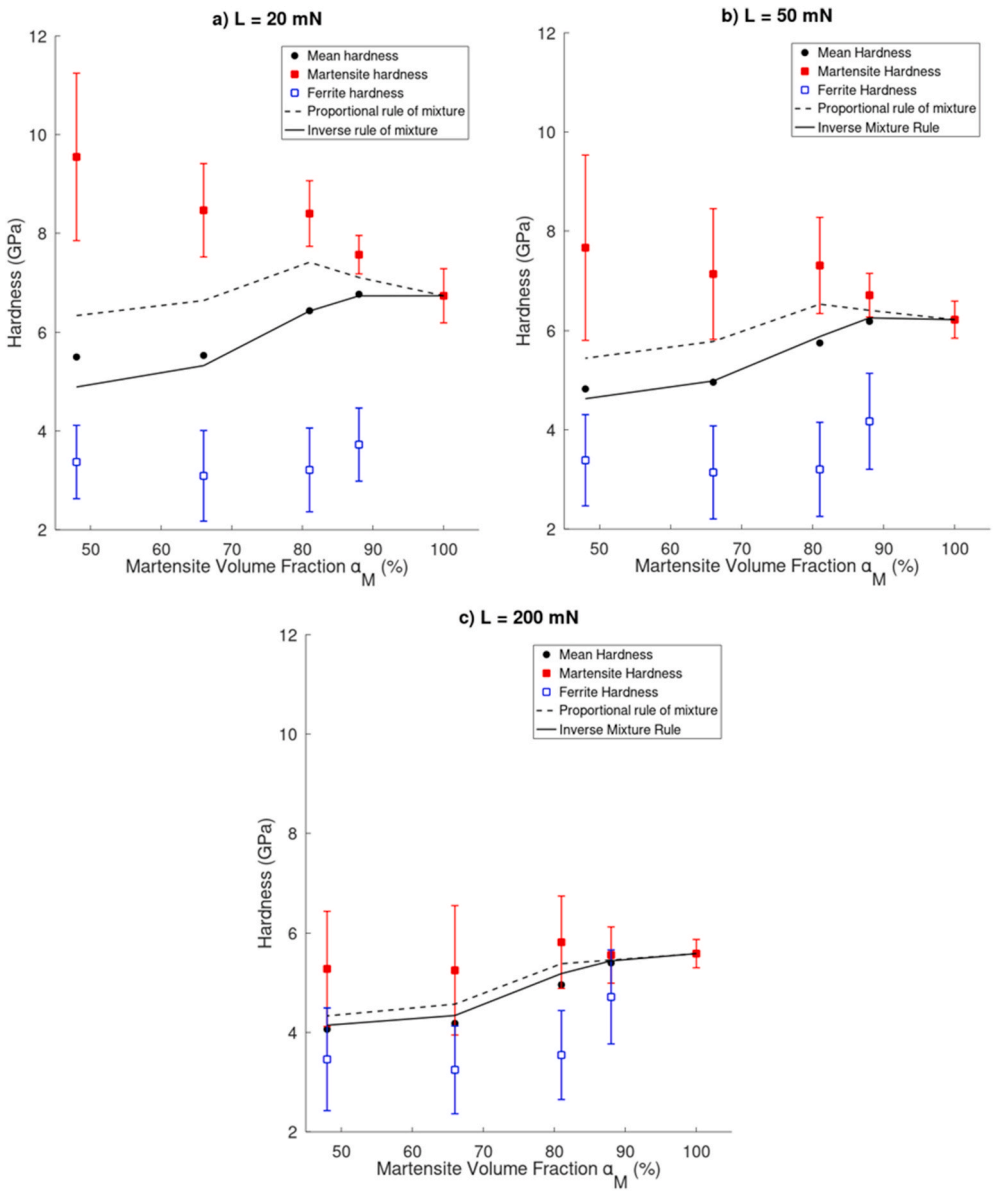

Fig. 6. Comparison between mean hardness and both proportional and inverse rule of mixture calculated from ferrite and martensite hardness at each martensite volume fraction for loads a) 20 mN, b) 50 mN and c) 200 mN.

by martensite proximity. Whatever the load and martensite volume fraction, martensite hardness is higher than ferrite.

It is well-known that martensite hardness depends on carbon content as shown in Krauss synthetic study [31]. From the theoretical carbon content of the samples calculated in Table 2, martensite hardness is expected to vary from at least 4.5 GPa for M-100% sample to near 8 GPa for DP-48%. On Fig. 6a), martensite hardness vary from 6.74 GPa to 9.55 GPa at 20 mN. These values are higher than those predicted from Krauss but the variation with carbon content is similar. The difference can be explained because of the indentation size effect (ISE). This ISE occurs because the number of dislocation is smaller when the volume of deformation is small, inducing the hardening of the material at low loads of indentation. On the other hand, at 200 mN martensite hardness is between 5 GPa and 6 GPa for all samples. In this case, ISE is reduced because of the increased volume of deformation and the value is closer to the macro-hardness of the phase. Moreover, for dual-phase microstructures, the size of indentation is close to the martensite grain size so martensite hardness is influenced by the surrounding ferrite, leading to a decrease in the measurement [32].

In order to better correlate the effect of ISE on the macro-hardness of the samples, the mean hardness from all measurements (ferrite and martensite) realized on each sample is represented as function of the depth of indentation in Fig. 7 for values obtained by Loubet analysis. Hardness calculations below 300 nm are not considered because of the tip defect and the maximum depth of indentation is 1.5 µm. For all samples, the mean hardness (represented as points) decreases as a function of depth of indentation and can be described by the model of Nix and Gao [30] as in equation (7) (dashed lines).

The macro-hardness H_0 and the characteristic length h* are calculated for both Oliver and Pharr and Loubet methods and compared to Vickers hardness in Table 3. It is shown that whatever the method, macro-hardness increases while the characteristic length decreases with martensite volume fraction. Nonetheless, a better agreement is found between Loubet method and Vickers hardness while Oliver and Pharr method overestimates by more than 1 GPa the macro-hardness values. It is known that Oliver and Pharr method overestimates the hardness of materials that form pile-up during indentation [33] because of the underestimation of the contact depth. Indeed, in equation (2), the contact

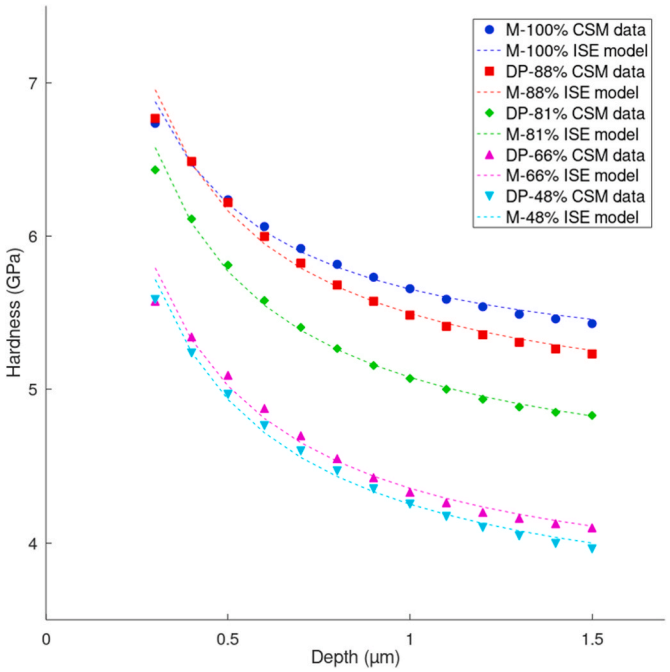

Fig. 7. Mean hardness as function of depth of indentation fitted by ISE model.

Table 3
Vickers hardness HV2 and calculated macrohardness H0 and characteristic length h* from ISE.

Sample	H0 (GPa) O&P	h* (nm) O&P	H0 (GPa) Loubet	h* (nm) Loubet	HV2 (GPa)
M-100%	6,77	167	5.04	258	5,02 ± 0,04
DP-88%	6,48	175	4.74	347	4,76 ± 0,06
DP-81%	5,77	355	4.28	409	4,52 ± 0,07
DP-66%	4,89	377	3.57	491	3,82 ± 0,26
DP-48%	4,72	420	3.44	530	3,62 ± 0,08

depth from the Oliver and Pharr method can only be smaller than the total depth, meaning that only sink-in can be represented. On the other hand, in the calculation of the contact depth from the Loubet method in equation (4), the sink-in or pile-up behaviors are possible depending on the value of the ratio H/E*. Sink-in is available for high H/E* value whereas pile-upis available for low value of H/E*. The values of the H/E* ratio suggest that martensite is subjected to sink-in whereas ferrite is subjected to pile-up. Indeed, on Fig. 2b) and c), pile-up is visible around the imprints for the ferrite phase. Moreover, the results validate the use of Loubet method for the analysis of hardness in this study. The evolution of macro-hardness of dual-phase steel with martensite volume fraction is often related to martensite and ferrite hardness through a proportional rule of mixture [34,35]:

$$H_0 = \alpha_M H_M + (1-\alpha_M) H_F \tag{8}$$

This equation suggests a linear relationship between dual-phase macro-hardness and martensite volume fraction. However, its reliability has been criticized by some authors because it supposes that the hardness of ferrite and martensite do not change with martensite volume fraction [36–38]. However, as shown in Fig. 6, martensite hardness vary greatly with its carbon content.

Then, the proportional rule of mixture considering constant properties of the individual phases is not consistent with the real martensite and ferrite properties. Moreover, as shown by the dashed lines on Fig. 6, introducing the varying properties of ferrite and martensite into the proportional rule of mixture leads to an overestimation of the mean hardness at low martensite volume fraction due to the increase in martensite hardness. A better agreement is obtained by proposing an inverse rule of mixture, shown on Fig. 6 by the plain lines:

$$H_0 = \left(\frac{\alpha_M}{H_M(\alpha_M)} + \frac{1-\alpha_M}{H_F(\alpha_M)} \right)^{-1} \tag{9}$$

This relation suggests that the almost linear behavior of the mean hardness is in fact due to the compensation of the nonlinear inverse rule of mixture by the variation of martensite hardness with martensite volume fraction. Moreover, an inverse rule of mixture suggests that as the martensite volume fraction decreases and the martensite hardness increases, the strain is confined mostly in the ferrite phase, implying that the macro-hardness becomes closer to ferrite hardness.

We have seen that martensite and ferrite hardness in dual-phase steels vary with martensite volume fraction and load and that these variations can be related to the macro-hardness of the sample through an inverse rule of mixture. The next section presents the friction and wear behavior of martensite and ferrite phases observed from the scratch tests.

3.2. Friction coefficient

Fig. 8 shows the evolution of the friction coefficient of the martensitic and ferritic phase as function of the tangent of the attack angle of the tip at different loads and for the five microstructures. Whatever the load, the microstructure and the phase considered, the friction coefficient increases with the attack angle. Moreover, friction coefficient in ferrite is higher than in martensite.

For a conical tip, the ploughing friction coefficient is usually expressed as:

$$\mu_p = 2/\pi tan\beta \tag{10}$$

This expression is also shown on Fig. 6 as a dashed line. We can observe that at a load of 200 mN, the friction coefficient for martensite is close to this ideal ploughing component while deviations are observed at lower loads. The deviations from linearity observed at 20 mN and 50 mN can be attributed to the tip defects. Indeed, at these loads, the scratch depth is below or close to 1 μm. The measured geometries have shown that tips are not perfectly conical at these depths so the friction coefficient is reduced compared to perfect conical tips. Then, we can suppose that martensite friction coefficient is close to the expression in equation (10) for conical tips. On the other hand, the higher friction coefficient of ferrite has to be explained by other means. Various authors have proposed expressions that had the effect of interfacial shear strength to the expression of the friction coefficient, either directly in the ploughing component of the friction or as an independent adhesive component [2,3,8]. In any case, an increase in the interfacial shear strength leads to an increase in the friction force and a higher friction coefficient. Then, an increased interfacial shear strength of ferrite compared to martensite could explain this higher friction coefficient. Another possibility is that in dual-phase microstructures, when the tip is ploughing through a ferrite grain, a harder martensite grain always contains the plastic deformation ahead of the tip, increasing the friction force.

Fig. 9 shows the evolution of the friction coefficient of the martensitic and ferritic phase as function of the martensite volume fraction for each tip and load. Similar variations are observed for martensite and ferrite. As the martensite volume fraction increases, a small increase of the friction coefficient is observed at 20 mN while the friction coefficient is almost constant at 200 mN. For martensite, the variation of the friction coefficient at low load can be explained by the increased hardness for lower martensite volume fraction. At 200 mN, we have seen that the variation of the measured hardness of martensite is

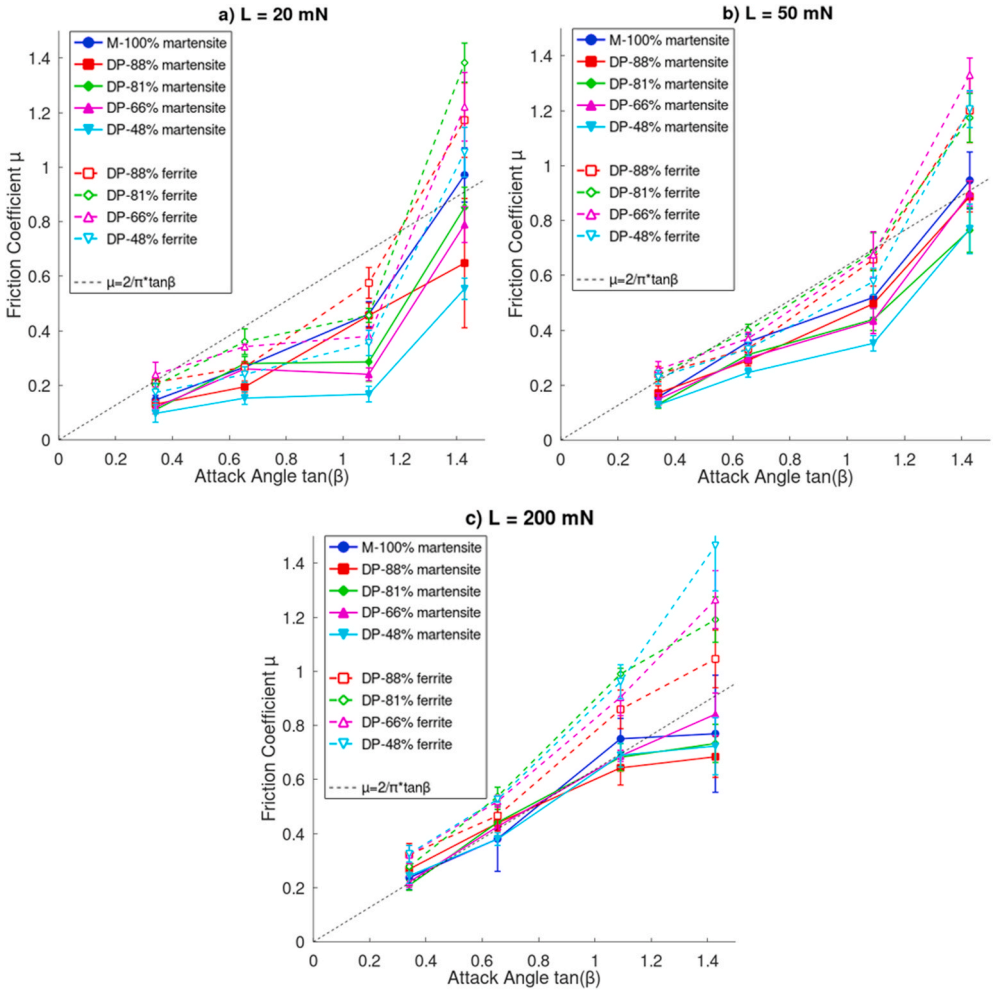

Fig. 8. Evolution of the friction coefficient as function of the attack angle for martensite and ferrite at a) 20 mN, b) 50 mN and c) 200 mN.

almost independent of the martensite volume fraction, due to the influence of the surrounding ferrite grains. Then, no variation of the friction coefficient on martensite are observed as martensite volume fraction varies. It is not the case for ferrite, for which the hardness is almost constant. However, if the deformation of the ferrite is limited by the surrounding martensite, this could lead to an increase of the friction force that depends on the martensite volume fraction and the load. Indeed, when martensite volume fraction increases, then ferrite grains are smaller and martensite contains more efficiently the plastic deformation of the ferrite. When the load increases, the volume of ferrite displaced is higher and more contained by the surrounding martensite.

3.3. Specific wear resistance

The classical formula that represent the wear rate of a material is the Archard's equation.

$$dV / dS = KL/H \tag{11}$$

where V is the volume loss, S is the sliding distance, L, the load, H the hardness of the worn material and K the wear coefficient that depends on material and contact properties. The specific wear resistance is defined as the ratio of H over K. For a scratch test, the wear rate dV/dS corresponds to the wear per unit scratch length and should be taken as the wear ratio f_{ab} defined in Fig. 10 multiplied by the cross-sectional area of the groove A_s.

In order to take into account the real geometry of the tips, in particular the tip defect, the scratch section is calculated as a function of the scratch depth directly from the mean profiles of each tip measured by AFM topography. On the other hand, the measurements of the wear ratio was not realized in this study so its value was taken as $f_{ab} = 1$. In consequence, the specific wear resistance is calculated as the ratio of the load to the calculated scratch section.

$$\Omega = H/K = L/A_s \tag{11a}$$

Fig. 11 represents the evolution of the specific wear resistance as function of the tip attack angle for martensite and ferrite. It is shown that whatever the load or the phase, the specific wear resistance decreases as the attack angle increases. Indeed, the specific wear resistance depends on the scratch section A_s, which is proportional to the groove width and the attack angle of the tip. Hence, under a given load and for a given hardness of the phase, the groove width should be constant whatever the tip while the depth increases in proportion to the attack angle. Then, the scratch section increases in proportion to the attack angle and the specific wear resistance decreases.

The evolution of specific wear resistance with martensite volume fraction can be observed on Fig. 12. Wear resistance of martensite decreases with martensite volume fraction at 20 and 50 mN while it is constant at 200 mN. Wear resistance of ferrite is constant whatever the martensite volume fraction and the load, while being lower than martensite wear resistance. Those variations are very similar to the variation of hardness of the phases, which is coherent with the definition of the specific wear resistance.

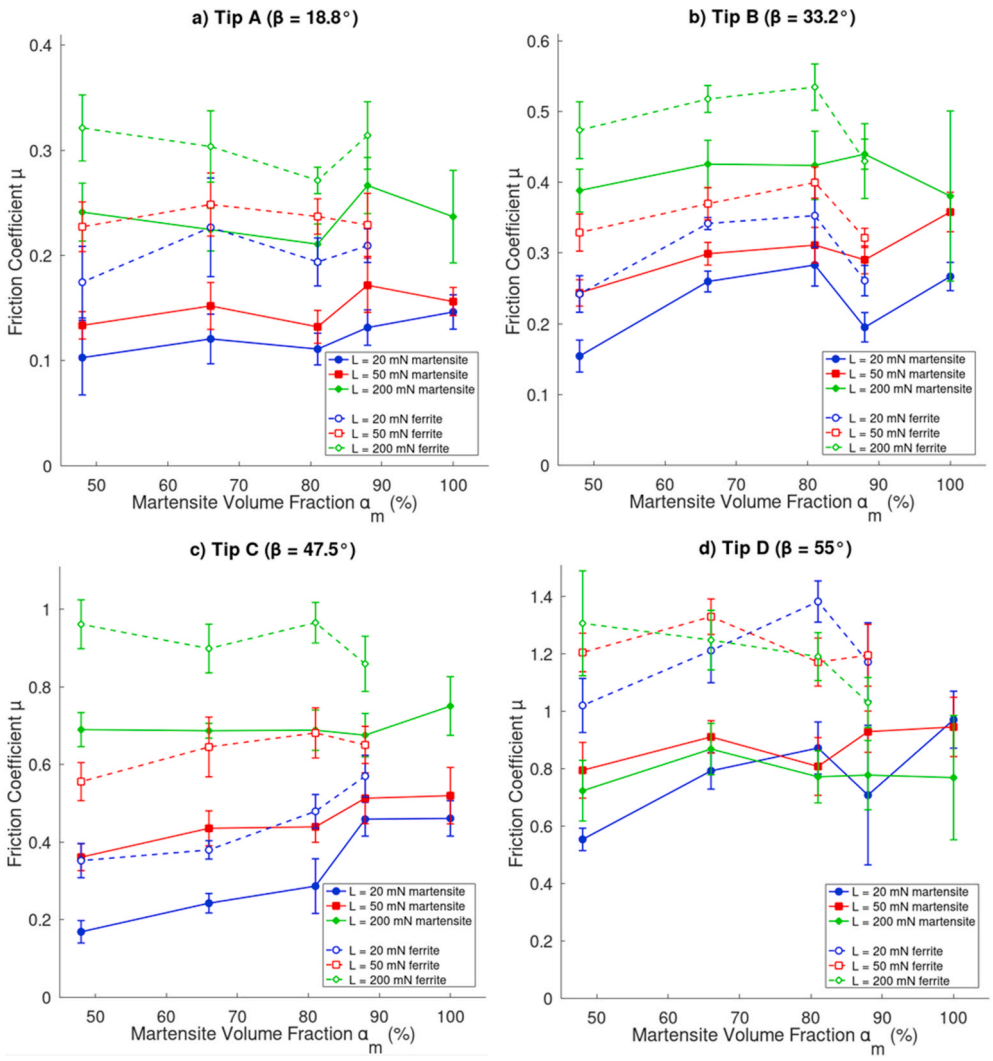

Fig. 9. Evolution of the friction coefficient as function of the martensite volume fraction for martensite and ferrite at each load with a) tip A (β = 18.8°), b) tip B (β = 33.2°), c) tip C (β = 47.5°) and d) tip D (β = 55°).

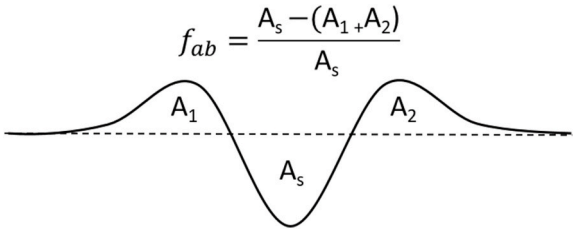

Fig. 10. Cross-sectional area of the wear groove and definition of the wear ratio f_{ab}.

3.4. Wear mechanisms

Fig. 13 shows SEM images of the scratches on samples M-100%, DP-81% and DP-48% for the four tips at a load of 50 mN. Hokkirigawa and Kato [11] have shown that the wear mechanism is dependent on the attack angle but also on the hardness of the material. As the attack angle increases, the wear mechanisms are ploughing, wedging and cutting. The critical attack angle for the transition between ploughing and wedging is independent of the hardness of the material while the critical attack angle for the transition between wedging and cutting decreases as hardness increases. Those results have been obtained from homogeneous materials and related to the macro-hardness. However, for dual-phase microstructures, we can observe on Fig. 13 that various wear mechanisms are present at the same time, depending on the tip attack angle and the worn phase. Then, a more precise analysis of the wear mechanisms at the micro-scale is needed to understand how each phase is worn. For the martensitic sample M-100%, the evolution of wear mechanisms is observed as the tip attack angle increases. For an attack angle of 18.8°, micro ploughing occurs and pile-up form on the edge of the groove. For an attack angle of 33.2°, the wear mechanism is wedging. Finally, for attack angles higher than 47.5°, micro cutting occurs with no or only small pile-up and the formation of micro-chips that are detached from the surface. For dual-phase microstructures, martensite behavior is similar to the homogeneous martensite, with a transition from ploughing to wedging and cutting while increasing the attack angle.

On the other hand, ferrite shows only micro-ploughing whatever the attack angle with the formation of pile-up on the side of the groove. However, the deformation of the ferrite is contained by surrounding martensite grains. When the deformation occurs close to the ferrite-martensite interface, the pile-up is forced upward over the martensite grain, leading to the formation of bigger pile-up or small chips.

Then, it seems that Hokkirigawa and Kato relations between wear mechanisms, hardness and tip attack angle are still mainly valid at the scale of each phase. However, the macroscopic behavior of multiphase

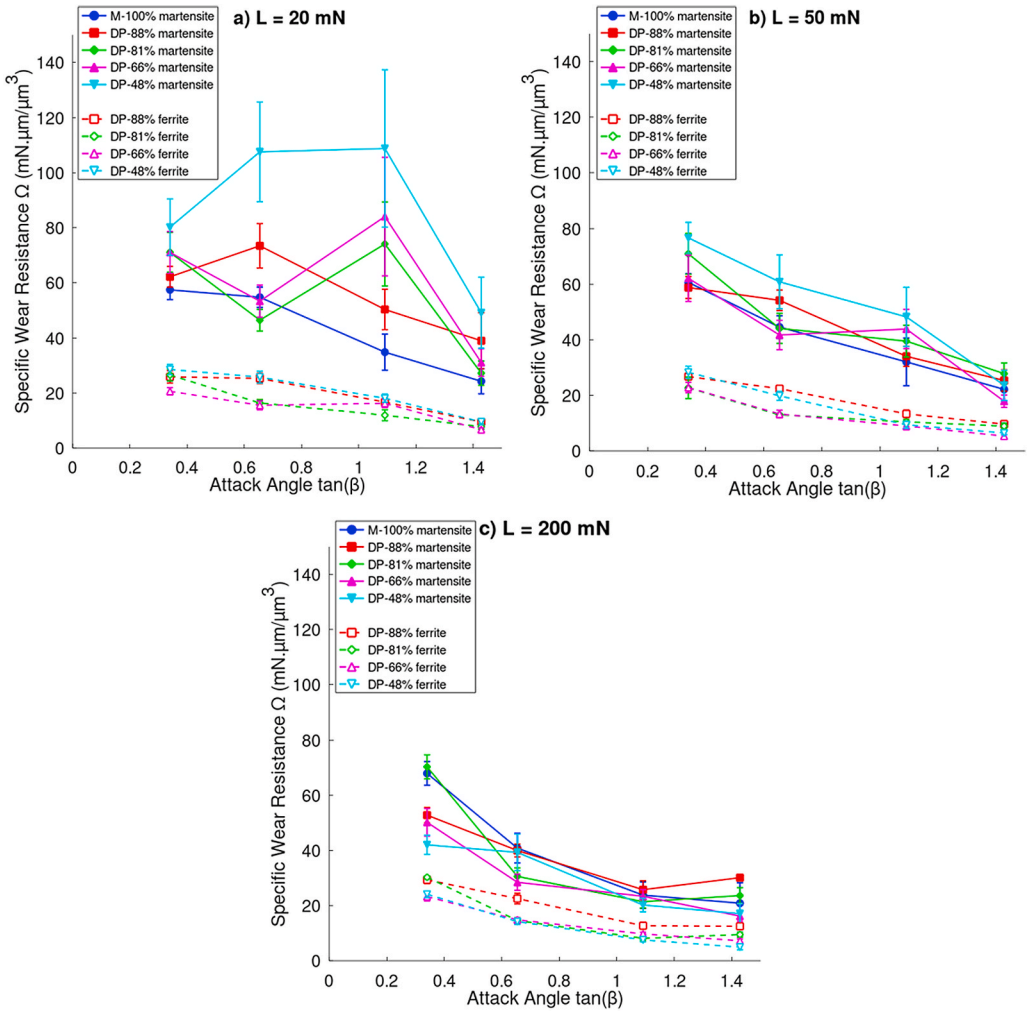

Fig. 11. Evolution of the specific wear resistance as function of the attack angle for martensite and ferrite at a) 20 mN, b) 50 mN and c) 200 mN.

materials is a complex combination between the wear mechanisms on each phase and can't be reduced to the macro-hardness. Then, the characterizations of the tribological behavior at the scale of each phase of a multi-phase material and in particular in dual-phase steels is important in order to understand the differences between various microstructures with similar macroscopic properties.

4. Modeling study

Study of the tribological behavior of martensite and ferrite phases has been realized. Correlation with martensite volume fraction has shown that the friction coefficient of both phases increases slightly at 20 mN and 50 mN or is constant at 200 mN when the fraction of martensite increases and that specific wear resistance follow the same trends as the hardness of the phases. In order to relate those individual phase behavior to the macroscopic tribological behavior of the dual-phase microstructures, two models for the friction and wear behavior of multiphase materials, initially proposed by Axén & al. are adapted and compared to experimental results [26,27]. The models are used to calculate the macroscopic specific wear resistance and friction coefficient from those of the isolated phases. However, in these original studies, the properties of the phases were considered constant with their volume fraction. We saw that in the case of dual-phase steel, hardness, friction coefficient and specific wear resistance vary with the martensite volume fraction, in particular for the martensitic phase. Hence, this section presents an adaptation of the models of Axén & al. which take into account these variations. Predictions from the models for dual-phase steel are compared to experimental results in the last section.

4.1. Model for the specific wear resistance

Axén et al. define the specific wear resistance from the Archard's equation which predicts the wear rate as function of the load and hardness. For homogeneous materials, the equation is:

$$\frac{dV}{dS} = K\frac{L}{H} \tag{13}$$

where V is the volume loss, S is the sliding distance, L is the normal load, H is the hardness of the worn material and K is the wear coefficient. From this equation, Axén et al. define the specific wear resistance Ω as the inverse of the specific wear rate κ, defined as the ratio between the wear coefficient K and the hardness H:

$$\Omega = 1/\kappa = H/K \tag{14}$$

Thus, the Archard's equation can be written:

$$\frac{dV}{dS} = \frac{L}{\Omega} \tag{15}$$

For a multiphase material, the wear rate is equal to the sum of the wear rate of each isolated phase, so we have the following relations:

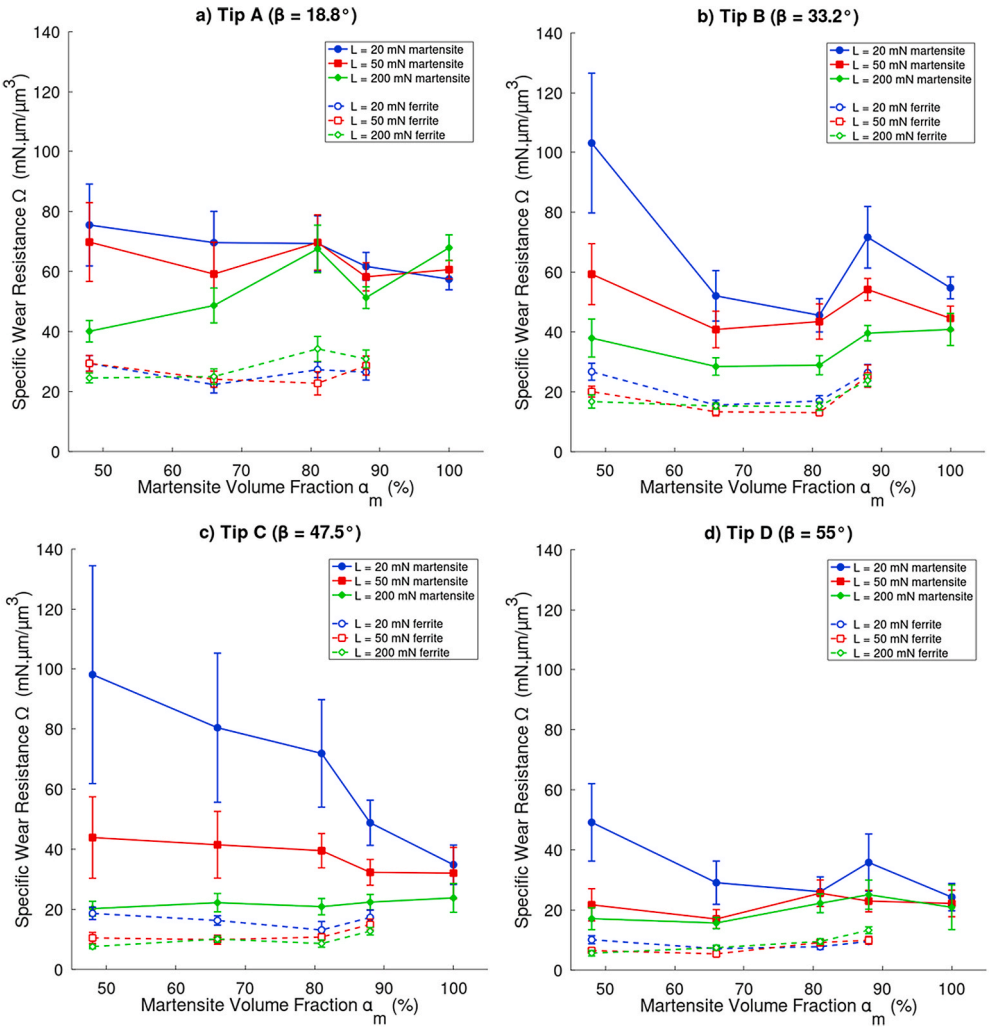

Fig. 12. Evolution of the specific wear resistance as function of the martensite volume fraction for martensite and ferrite at load 20 mN, 50 mN and 200 mN for a) tip A (β = 18.8°), b) tip B (β = 33.2°), c) tip C (β = 47.5°) and d) tip D (β = 55°).

$$\frac{dV}{dS} = \sum_{i}^{N} \frac{dV_i}{dS} \tag{16}$$

$$\frac{L}{\Omega} = \sum_{i}^{N} \frac{L_i}{\Omega_i} \tag{17}$$

In the case of ferrite-martensite dual-phase microstructures, only two terms corresponding to the martensite phase (i = M) and the ferrite phase (i = F) are needed:

$$\frac{dV}{dS} = \frac{dV_M}{dS} + \frac{dV_F}{dS} \tag{18}$$

$$\frac{L}{\Omega} = \frac{L_M}{\Omega_M} + \frac{L_F}{\Omega_F} \tag{19}$$

Finally, the volumetric wear rate can also be written as the product of the linear wear rate, defined as the variation of scratch depth h with the sliding distance S and the nominal contact area A as follows:

$$\frac{dh}{dS}A = \frac{dh_M}{dS}A_M + \frac{dh_F}{dS}A_F \tag{20}$$

Based on these equations of the specific wear resistance, Axén et al. develop two different wear modes derived from two different sets of assumptions on the pressure and wear distribution between the phases.

The first mode, called the Equal Wear (EW) mode, considers that the isolated phases are worn at the same rate, equal to the wear rate of the material. Written in term of the linear wear rates, this assumption leads to the following equality:

$$\frac{dh}{dS} = \frac{dh_M}{dS} = \frac{dh_F}{dS} \tag{21}$$

Introducing to the previous equations, that gives:

$$\frac{dh}{dS}A = \frac{dh}{dS}A_M + \frac{dh}{dS}A_F \tag{22}$$

Using equation (15), we get:

$$\frac{dh}{dS}A = \frac{L}{\Omega} \tag{23}$$

$$\frac{dh}{dS}A_M = \frac{L_M}{\Omega_M} \tag{24}$$

$$\frac{dh}{dS}A_F = \frac{L_F}{\Omega_F} \tag{25}$$

Combining equations (24) and (25), we obtain the relations:

$$\frac{L_M}{\Omega_M A_M} = \frac{L_F}{\Omega_F A_F} \tag{26}$$

$$L_M = L_F \frac{\Omega_M A_M}{\Omega_F A_F} \tag{27}$$

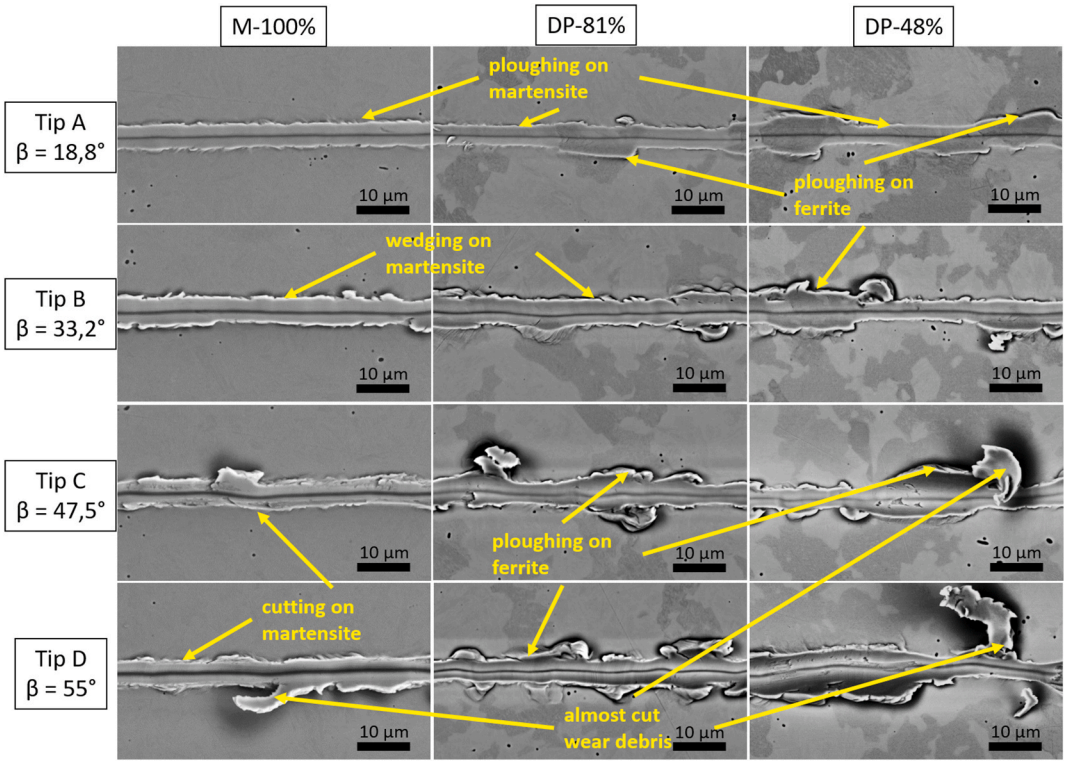

Fig. 13. SEM images of scratches realized at a load of 50 mN with tips A-D on samples M-100%, DP-81% and DP-48%.

In this mode, the pressure is not carried by each phase in proportion of their volume fraction. However, the total load is still the sum of the load carried by each phase:

$$L = L_M + L_F \tag{28}$$

Combining equations (27) and (28), we obtain the expressions of the load carried by the martensitic and ferritic phase:

$$L_M = L\frac{\Omega_M A_M}{\Omega_M A_M + \Omega_F A_F} \tag{29}$$

$$L_F = L\frac{\Omega_F A_F}{\Omega_M A_M + \Omega_F A_F} \tag{30}$$

Finally, incorporating equations (29) and (30) into equation (19), we get the expression of the specific wear resistance as described by the EW mode:

$$\Omega_{EW} = \alpha_M \Omega_M + \alpha_F \Omega_F \tag{31}$$

where $\alpha_M = A_M/A$ and $\alpha_F = A_F/A$ are the volume fractions of martensitic and ferritic phases respectively. Considering that $\alpha_F = 1 - \alpha_M$, equation (31) can be rewritten:

$$\Omega_{EW} = \alpha_M \Omega_M + (1 - \alpha_M)\Omega_F \tag{32}$$

This mode describes an ideal case where the dual-phase material benefits fully from its reinforcing phase, maximizing the specific wear resistance. Considering that the specific wear resistance of the isolated phases are constant, the EW mode predicts a linear increase of the global specific wear resistance with volume fraction of martensite. However, as seen in the experimental results of this study, the specific wear resistances of martensite and ferrite phases are not constants with the martensite volume fraction, so the variations of the predicted specific wear resistance by EW mode should be more complex in the case of dual-phase steels.

The second mode considers that the pressure is equally supported by both phases, and so is called the Equal Pressure (EP) mode. This assumption is translated into the following equations:

$$L_M = \alpha_M L \tag{33}$$

$$L_F = \alpha_F L \tag{34}$$

Then, introducing equations (33) and (34) into equation (19), we can write the specific wear resistance as described by the EP mode:

$$\Omega_{EP} = \left(\frac{\alpha_M}{\Omega_M} + \frac{\alpha_F}{\Omega_F}\right)^{-1} \tag{35}$$

Finally, considering that $\alpha_F = 1 - \alpha_M$, we get:

$$\Omega_{EP} = \left(\frac{\alpha_M}{\Omega_M} + \frac{1 - \alpha_M}{\Omega_F}\right)^{-1} \tag{36}$$

This mode describes the case where the hard martensitic phase does not protect the soft ferritic phase and so minimizes the specific wear resistance of the dual-phase steel. The relation between the specific wear resistances of the phases and the one of the dual-phase material is an inverse rule of mixture similar to the one identified for the evolution of hardness as a function of the martensite volume fraction.

4.2. Model for the friction coefficient

Axén et al. also proposed relations for the modelization of the friction coefficient of multiphase materials based on the same two EW and EP modes. The models are formulated considering the relation between the tangential friction force T, the normal load L and the friction coefficient μ:

$$T = \mu L \tag{37}$$

By making the hypothesis that the phases present distinct friction properties, the formula can be written for the isolated phases of the dual-phase steel:

$$T_M = \mu_M L_M \tag{38}$$

$$T_F = \mu_F L_F \tag{39}$$

Considering that the total tangential friction force is the sum of the tangential friction force on each phase, we can write:

$$T = T_M + T_F \tag{40}$$

$$T = \mu_M L_M + \mu_F L_F \tag{41}$$

Then, the expression of the load carried by each phase described for the EW and EP modes can be introduced in order to obtain the expression of the friction coefficient for each mode.

For the EW mode, the load carried by each phase are expressed in equations (29) and (30) and introduced into equation (41), giving the expression of the tangential friction force for EW mode:

$$T_{EW} = \mu_M L \frac{\Omega_M A_M}{\Omega_M A_M + \Omega_F A_F} + \mu_F L \frac{\Omega_F A_F}{\Omega_M A_M + \Omega_F A_F} \tag{42}$$

Finally, introducing $\mu_{EW} = T_{EW}/L$, $\alpha_M = A_M/A$ and $\alpha_F = A_F/A = 1 - \alpha_M$, we obtain the expression of the friction coefficient predicted by the EW mode:

$$\mu_{EW} = \frac{\alpha_M \mu_M \Omega_M + (1-\alpha_M)\mu_F \Omega_F}{\alpha_M \Omega_M + (1-\alpha_M)\Omega_F} \tag{43}$$

Then, in the EW mode, the friction coefficient of the dual-phase microstructure depends on the volume fraction, the friction properties and the specific wear resistance of both phases.

Considering equations (33) and (34) for the load carried by the phases in the EP mode and combining them with equation (41), the tangential friction force for EP mode is:

$$T_{EP} = \mu_M L \alpha_M + \mu_F L \alpha_F \tag{44}$$

So with $\mu_{EP} = T_{EP}/L$ and $\alpha_F = 1 - \alpha_M$, equation (44) becomes:

$$\mu_{EP} = \alpha_M \mu_M + (1-\alpha_M)\mu_F \tag{45}$$

In the EP mode, the friction coefficient depends only on the volume fraction and the friction properties of the phases but not on their specific wear resistances. Considering that the friction coefficient of the isolated phases are constant, the EP mode predicts a linear increase of the global friction coefficient with volume fraction of martensite. However, as seen in the experimental results of this study, the friction coefficients of martensite and ferrite phases are not constants with the martensite volume fraction, so the variations of the predicted global friction coefficient by EP mode should be more complex in the case of dual-phase steels.

5. Comparison between experimental and modeling results

Fig. 14 and Fig. 15 present respectively the experimental mean

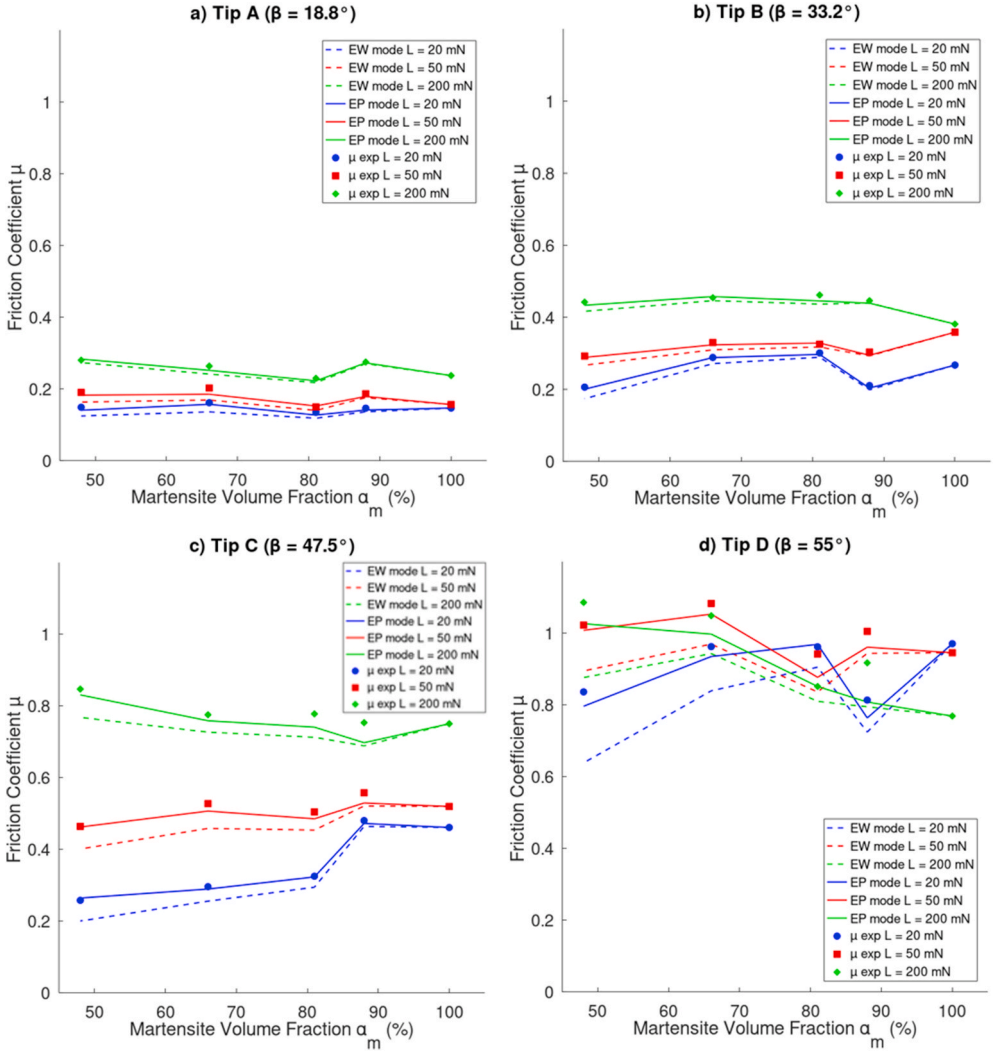

Fig. 14. Comparison between experimental friction coefficient and calculated EP and EW model at load 20 mN, 50 mN and 200 mN for a) tip A (β = 18.8°), b) tip B (β = 33.2°), c) tip C (β = 47.5°) and d) tip D (β = 55°).

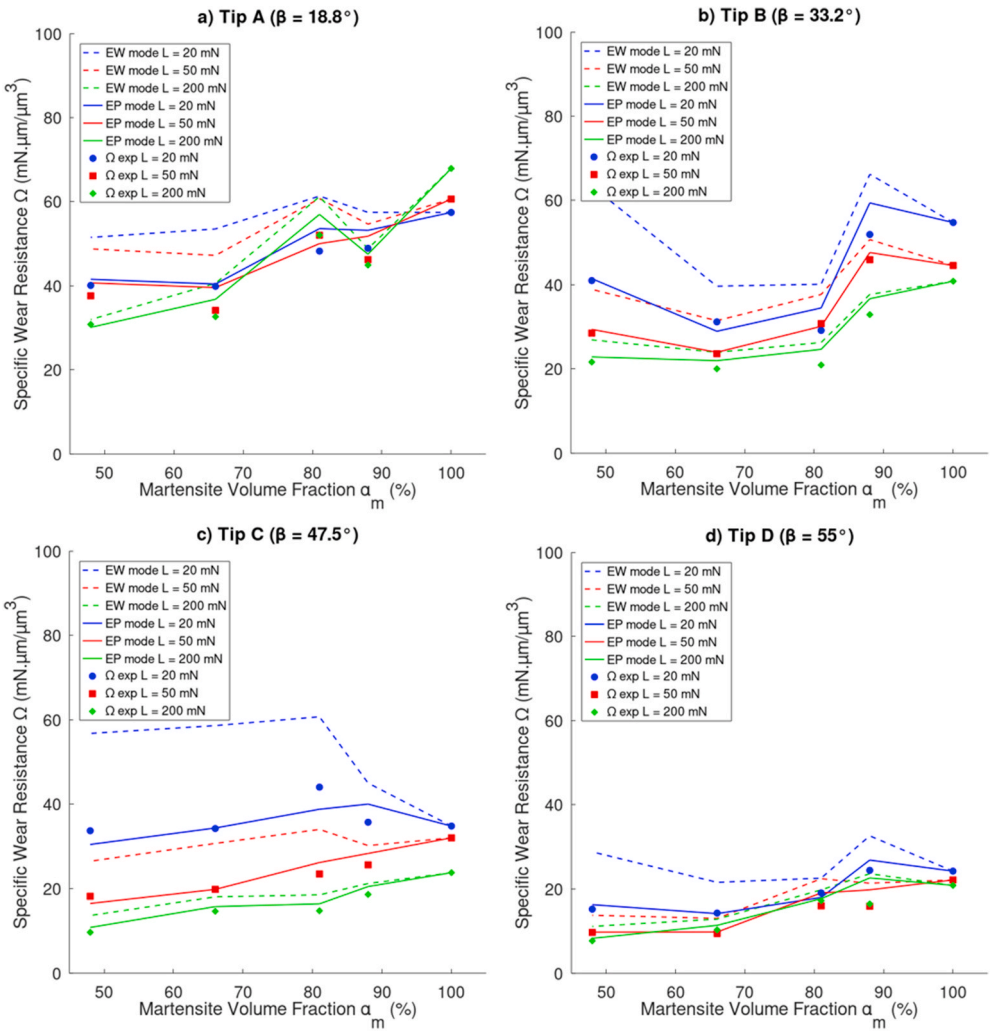

Fig. 15. Comparison between experimental specific wear resistance and calculated EP and EW model at load 20 mN, 50 mN and 200 mN for a) tip A (β = 18.8°), b) tip B (β = 33.2°), c) tip C (β = 47.5°) and d) tip D (β = 55°).

friction coefficient and mean specific wear resistance obtained from each scratch tests. Those mean values are calculated directly from the measured profiles for each scratch presented in Fig. 4 without differentiation between ferrite and martensite. Each scratch profile has a length of 500 µm and a resolution of 1 point/µm so the calculated means are the averages of 500 points.

These results are compared to EW and EP modes calculated from the friction coefficient and specific wear resistance measured on individual ferrite and martensite phases and presented in previous sections. It is clearly demonstrated that in the case of pure abrasion tests, the pressure distribution mode that best describes the dual-phase microstructure behavior is the EP mode.

Conclusions similar to the inverse rule of mixture proposed for calculating the macro-hardness of the dual-phase microstructure can be done with the EP mode. Indeed, the specific wear resistance should be proportional to hardness. It is then not surprising that an inverse rule of mixture between the specific wear resistance of martensite and ferrite, like the EP mode in this case, corresponds to the behavior of this dual-phase steel.

Trevisiol & al [16]. have studied the tribological behavior of dual-phase steels in light of Axén et al. model at a macro scale. They have observed that for coarse abrasive particles, the associated pressure distribution is best described by the EP mode while for fine abrasive particles, the EW mode is better. Jourani & al [39]. have observed a transition in the friction coefficient behavior between fine particles and coarse particles. In terms of wear mechanisms, coarse particles are associated with mainly abrasive wear while fine particles are associated with an increased adhesive wear. In comparison, scratch tests simulate the behavior of abrasive wear only. Then, it can be concluded that EP mode is adapted to describe the behavior of dual-phase microstructure if abrasive wear is dominant while deviations are to be expected if adhesive wear increases.

Moreover, another interesting feature is observed concerning the evolution of friction coefficient and specific wear resistance in order to optimize the microstructure. Indeed, the optimal martensite volume fraction is not the same as the load increases. For specific wear resistance, whatever the tip and load, the fully martensitic microstructure always presents the highest value. This trends could mean that the specific wear resistance is mostly governed by the martensite volume fraction, or the macro-hardness. On the other hand, the minimal friction coefficient is obtained at 48% martensite at 20 mN and 50 mN while it is obtained at 100% martensite at 200 mN. Then the increased hardness of the martensite at low martensite volume fraction leads to an improvement of the friction coefficient of dual-phase microstructures even though ferrite presenting a higher friction coefficient is also present. This improvement is significant until the load is sufficiently high for the martensite hardness to be influenced by surrounding ferrite.

6. Conclusion

Scratch tests realized on ferrite-martensite microstructures allows to study the effect of martensite volume fraction, normal load and attack angle on individual phase hardness, friction, wear resistance and wear mechanisms. Dual-phase microstructures with martensite volume fraction from 48% to 100% are obtained from a step quenched heat treatment. Nanoindentation hardness is measured on ferritic and martensitic phases. Scratch tests are realized with conical tips with attack angle from 18.8° to 55° at loads from 20 mN to 200 mN. Experimental results are compared to the friction and wear models for multiphase materials proposed by Axén & al. in order to determine the pressure distribution mode. Main results of this work are:

- Martensite hardness decreases with its carbon content while ferrite hardness is constant with martensite volume fraction. When the load increases, an indentation size effect is identified for each sample and the corresponding macro-hardness is calculated. Whatever the load, macro hardness increases with martensite volume fraction, showing a good agreement with an inverse rule of mixture between individual phases hardness. Finally, it is demonstrated that the Loubet method of analysis for nanoindentation data better agrees to Vickers microhardness on dual-phase steel than the more common Oliver & Pharr method.
- Whatever the martensite volume fraction, friction coefficient of martensite agrees well with the theoretical ploughing friction coefficient $\mu_p = \frac{2}{\pi}\tan(\beta)$ where β is the attack angle of the conical tip. On the other hand, friction coefficient of ferrite is always higher than this value, suggesting a higher resistance to ploughing. Increasing the hardness of martensite at low martensite volume fraction leads to a small decrease in the friction coefficient.
- For a given hardness of a phase, specific wear resistance decreases when the attack angle increases, corresponding to an increased groove volume for similar groove width. Moreover, specific wear resistance of martensite decreases with martensite volume fraction while specific wear resistance of ferrite is constant and lower than martensite. Those variations suggests that for a given geometry of asperity, the specific wear resistance is mainly influenced by hardness of the phase.
- Whatever the tip geometry and martensite volume fraction, wear mechanisms is always ploughing for ferrite. On the other hand, martensite shows a transition from ploughing followed by wedging and cutting when the tip attack angle increases from 18.8° to 55°.
- The variation of friction coefficient and specific wear resistance of martensite and ferrite are implemented in the models for multiphase materials of Axén & al. Results show that the model of equal pressure hypothesis applies well to the scratch tests on dual-pase steel.
- This work applies on the friction and wear behaviors of the material in its 'virgin' state. In practical situation, the tribological behavior is expected to go from a run-in to a steady-state behavior. Further studies will have to extend the results presented in this paper to the situation where the microstructure is scratched multiple times until a steady-state is attained.

Declaration of competing interest

The authors declare that they have no known competing financial interests or personal relationships that could have appeared to influence the work reported in this paper.

References

[1] K.H.Z. Gahr, Wear by hard particles, Tribol. Int. 31 (10) (1998) 587–596.
[2] J. Goddard, H. Wilman, A theory of friction and wear during the abrasion of metals, Wear 5 (1961) 114–135.
[3] H. Sin, N. Saka, N.P. Suh, Abrasive wear mechanisms and the grit size effect, Wear 55 (1) (1979) 163–190.
[4] A. Jourani, B. Hagège, S. Bouvier, M. Bigerelle, H. Zahouani, Influence of abrasive grain geometry on friction coefficient and wear rate in belt finishing, Tribol. Int. 59 (2013) 30–37.
[5] I. Alabd Alhafez, A. Brodyanski, M. Kopnarski, H.M. Urbassek, Influence of tip geometry on nanoscratching, Tribol. Lett. 65 (1) (2017) 1–13.
[6] M. Barge, G. Kermouche, P. Gilles, J.M. Bergheau, Experimental and numerical study of th ploughing part of abrasive wear, Wear 255 (1–6) (2003) 30–37.
[7] J.L. Bucaille, E. Felder, G. Hochstetter, Mechanical analysis of the scratch test on elastic perfectly plastic materials with the three-dimensional finite element modeling, Wear 249 (5–6) (2001) 422–432.
[8] G. Subhash, W. Zhang, Investigation of the overall friction coefficient in single-pass scratch test, in: ", vol. 252, 2002, pp. 123–134. September 2001.
[9] N. Cane, J. Skinner, The friction and scratch deformation of metals on a micro scale 24 (1973) 207–217.
[10] J.F. Archard, Contact and rubbing of flat surfaces, J. Appl. Phys. 24 (8) (1953) 981–988.
[11] K. Hokkirigawa, K. Kato, Z.Z. Li, The effect of hardness on the transition of the abrasive wear mechanism of steels, Wear 123 (2) (1988) 241–251.
[12] S. Mezlini, M. Zidi, H. Arfa, M. Ben Tkaya, P. Kapsa, Experimental, numerical and analytical studies of abrasive wear: correlation between wear mechanisms and friction coefficient, Compt. Rendus Mec. 333 (11) (2005) 830–837.
[13] M. Woldman, E. Van Der Heide, T. Tinga, M.A. Masen, The influence of abrasive body dimensions on single asperity wear, Wear 301 (1–2) (2013) 76–81.
[14] C. Trevisiol, A. Jourani, S. Bouvier, Effect of martensite morphology on tribological behavior of a low-alloy steel, Metallogr. Microstruct. Anal. 8 (1) (2019) 123–134.
[15] C. Trevisiol, A. Jourani, S. Bouvier, Effect of hardness, microstructure, normal load and abrasive size on friction and on wear behavior of 35NCD16 steel, Wear 388–389 (May) (2017) 101–111.
[16] C. Trevisiol, A. Jourani, S. Bouvier, Experimental study and modelling of the effect of microstructure on friction and wear mechanisms of low alloy steel, Mater. Res. Express 4 (12) (2017).
[17] C. Trevisiol, A. Jourani, S. Bouvier, Effect of martensite volume fraction and abrasive particles size on friction and wear behavior of a low alloy steel, Tribol. Int. 113 (2017) 411–425. July 2016.
[18] C. Trevisiol, A. Jourani, S. Bouvier, Effect of microstructures with the same chemical composition and similar hardness levels on tribological behavior of a low alloy steel, Tribol. Int. 127 (June) (2018) 389–403.
[19] H. Saghafian, S. Kheirandish, Correlating microstructural features with wear resistance of dual phase steel, Mater. Lett. 61 (14–15) (2007) 3059–3063.
[20] O.P. Modi, P. Pandit, D.P. Mondal, B.K. Prasad, A.H. Yegneswaran, A. Chrysanthou, High-stress abrasive wear response of 0.2% carbon dual phase steel: effects of microstructural features and experimental conditions, Mater. Sci. Eng., A 458 (1–2) (2007) 303–311.
[21] A.P. Modi, Effects of microstructure and experimental parameters on high stress abrasive wear behavior of a 0.19 wt% C dual phase steel, Tribol. Int. 40 (3) (2007) 490–497.
[22] V. Abouei, H. Saghafian, S. Kheirandish, Dry sliding oxidative wear in plain carbon dual phase steel, J. Iron Steel Res. Int. 14 (4) (2007) 43–48.
[23] R. Tyagi, S.K. Nath, S. Ray, Effect of martensite content on friction and oxidative wear behavior of 0.42 Pct carbon dual-phase steel, Metall. Mater. Trans. A Phys. Metall. Mater. Sci. 33 (11) (2002) 3479–3488.
[24] X. Xu, S. van der Zwaag, W. Xu, The effect of martensite volume fraction on the scratch and abrasion resistance of a ferrite-martensite dual phase steel, Wear 348–349 (2016) 80–88.
[25] X. Xu, S. Van der Zwaag, W. Xu, The effect of ferrite-martensite morphology on the scratch and abrasive wear behavior of a dual phase construction steel, Wear 348–349 (2016) 148–157.
[26] N. Axén, S. Jacobson, A model for the abrasive wear resistance of multiphase materials, Wear 174 (1–2) (1994) 187–199.
[27] N. Axén, I.M. Hutchings, S. Jacobson, A model for the friction of multiphase materials in abrasion, Tribol. Int. 29 (6) (1996) 467–475.
[28] W.C. Oliver, G.M. Pharr, An improved technique for determining hardness and elastic modulus using load and displacement sensing indentation experiments, J. Mater. Res. 7 (6) (1992) 1564–1583.
[29] B.G.-M.L. Loubet, M. Bauer, A. Tonck, S. Bec, Nanoindentation with a Surface Force Apparatus, 1993.
[30] W.D. Nix, H. Gao, Indentation size effects in crystalline materials: a law for strain gradient plasticity, J. Mech. Phys. Solid. 46 (3) (1998) 411–425.
[31] G. Krauss, Martensite in steel: strength and structure, Mater. Sci. Eng., A 273–275 (1999) 40–57.
[32] M. Delincé, P.J. Jacques, T. Pardoen, Separation of size-dependent strengthening contributions in fine-grained Dual Phase steels by nanoindentation, Acta Mater. 54 (12) (2006) 3395–3404.
[33] W.C. Oliver, G.M. Pharr, Measurement of hardness and elastic modulus by instrumented indentation: advances in understanding and refinements to methodology, J. Mater. Res. 19 (1) (2004) 3–20.
[34] H. Ashrafi, M. Shamanian, R. Emadi, N. Saeidi, Correlation of tensile properties and strain hardening behavior with martensite volume fraction in dual-phase steels, Trans. Indian Inst. Met. 70 (6) (2017) 1575–1584.
[35] Y. Mazaheri, A. Kermanpur, A. Najafizadeh, Strengthening mechanisms of ultrafine grained dual phase steels developed by new thermomechanical processing 55 (1) (2015) 218–226.
[36] E. Fereiduni, S.S. Ghasemi Banadkouki, Reliability/unreliability of mixture rule in a low alloy ferrite-martensite dual phase steel, J. Alloys Compd. 577 (2013) 351–359.

[37] F. Zhang, A. Ruimi, P.C. Wo, D.P. Field, Morphology and distribution of martensite in dual phase (DP980) steel and its relation to the multiscale mechanical behavior, Mater. Sci. Eng., A 659 (2016) 93–103.

[38] Y. Mazaheri, A. Kermanpur, A. Najafizadeh, Nanoindentation study of ferrite-martensite dual phase steels developed by a new thermomechanical processing, Mater. Sci. Eng., A 639 (2015) 8–14.

[39] A. Jourani, S. Bouvier, Friction and wear mechanisms of 316L stainless steel in dry sliding contact: effect of abrasive particle size, Tribol. Trans. 58 (1) (2015) 131–139.